ACS Partner Journal

CHEMICAL & BIOMEDICAL IMAGING

pubs.acs.org/ChemBioImaging

Article

FRET Imaging of Nonuniformly Distributed DNA SAMs on Gold Reveals the Role Played by the Donor/Acceptor Ratio and the Local Environment in Measuring the Rate of Hybridization

Adrian Jan Grzędowski, Tianxiao Ma, and Dan Bizzotto*

Cite This: *Chem. Biomed. Imaging* 2023, 1, 286–296

Read Online

ACCESS | Metrics & More | Article Recommendations | Supporting Information

ABSTRACT: Mixed DNA SAMs labeled with a fluorophore (either AlexaFluor488 or AlexaFluor647) were prepared on a single crystal gold bead electrode using potential-assisted thiol exchange and studied using Förster resonance energy transfer (FRET). A measure of the local environment of the DNA SAM (e.g., crowding) was possible using FRET imaging on these surfaces since electrodes prepared this way have a range of surface densities (Γ_{DNA}). The FRET signal was strongly dependent on Γ_{DNA} and on the ratio of AlexaFluor488 to AlexaFluor647 used to make the DNA SAM, which were consistent with a model of FRET in 2D systems. FRET was shown to provide a direct measure of the local DNA SAM arrangement on each crystallographic region of interest providing a direct assessment of the probe environment and its influence on the rate of hybridization. The kinetics of duplex formation for these DNA SAMs was also studied using FRET imaging over a range of coverages and DNA SAM compositions. Hybridization of the surface-bound DNA increased the average distance between the fluorophore label and the gold electrode surface and decreased the distance between the donor (D) and acceptor (A), both of which result in an increase in FRET intensity. This increase in FRET was modeled using a second order Langmuir adsorption rate equation, reflecting the fact that both D and A labeled DNA are required to become hybridized to observe a FRET signal. The self-consistent analysis of the hybridization rates on low and high coverage regions on the same electrode showed that the low coverage regions achieved full hybridization 5× faster than the higher coverage regions, approaching rates typically found in solution. The relative increase in FRET intensity from each region of interest was controlled by manipulating the donor to acceptor composition of the DNA SAM without changing the rate of hybridization. The FRET response can be optimized by controlling the coverage and the composition of the DNA SAM sensor surface and could be further improved with the use of a FRET pair with a larger (e.g., > 5 nm) Förster radius.

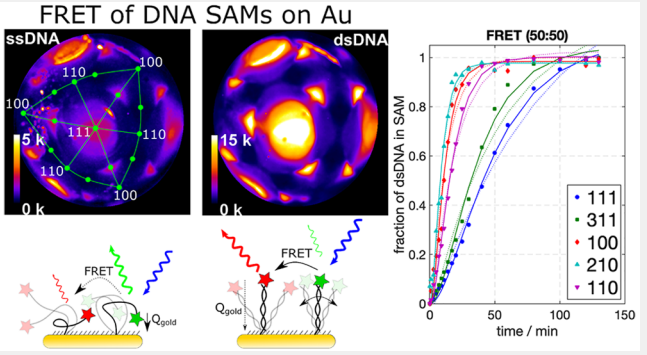

KEYWORDS: *fluorescence imaging, FRET imaging, DNA SAM modified electrodes, DNA surface hybridization, spectroelectrochemistry*

INTRODUCTION

The detection of biomolecules using functionalized surfaces has been realized using optical and/or electrochemical methods.[1−9] Sensors using nucleic acids as the surface-bound probes have been successful in the detection of a variety of analytes, from DNA and small molecules to proteins.[2,7,10,11] One common approach is to prepare a DNA self-assembled monolayer (SAM) via a thiol bond to the gold. The tethered DNA probe can be single stranded DNA (ssDNA), an aptamer, or a DNA hairpin. Electrochemical measurement of these SAMs involves an electron transfer reaction of the redox active label on the probe (e.g., methylene blue or ferrocene). Binding of the complementary strand (cDNA) or analyte will result in a change in the electron transfer characteristics.[12−16] The performance of the sensor strongly depends on the characteristics of the surface probe density, surface morphology or roughness, prevention of nonspecific adsorption, and the local environment or crowding around each tethered DNA probe (ssDNA, hairpin or aptamer).[12,13,15,17−19] Target interaction with the immobilized ssDNA probe and hybridization on the surface results in DNA structural rearrangement. This requires sufficient space around the probe or minimal crowding, achieved with a small average probe surface density,[17−20] assuming a uniformly distributed probe.

DNA hybridization with a surface-bound probe was shown to be significantly slower than solution based hybridization

Received: March 3, 2023
Revised: April 18, 2023
Accepted: May 5, 2023
Published: May 22, 2023

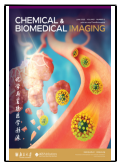

https://doi.org/10.1021/cbmi.3c00031
Chem. Biomed. Imaging 2023, 1, 286–296

events, as the DNA modified surface can have a high effective probe concentration not typically realized in the solution.[17,20−24] For ssDNA probes, the probe density and local environment plays a fundamental role, with a more densely packed layer tending to have significantly slower hybridization kinetics.[17,20,21] Hybridization rate is generally slower than in the solution and also varies greatly with more complex DNA structures assembled onto the surface (e.g., hairpins with duplexed regions, and those including overhangs).[21,23,25] This has been characterized with in situ single molecule AFM[26] for hairpin DNA SAMs, showing that the nearest-neighbor distances correlate with DNA hybridization rates. Although in some cases where clusters of DNA hairpins were observed, the hybridization rate increased due to increased destabilization of the hairpin.

Surface-based sensing can have many nonideal characteristics which further complicate sensing. The assembly of the probe on the surface should not result in the presence of aggregates, clusters, or nonspecifically adsorbed (e.g., adsorbed via phosphate backbone and not specifically via the thiol) probes.[19,27,28] The electrode surface may have defects which can affect the probe assembly, or the surface may be purposefully roughened to increase the number of adsorbed probes and increase their availability to bind with the target in solution.[29,30] Also, careful precleaning and pretreatment of the gold electrode surface is required to realize reproducible measurements. A number of methods for preparing DNA SAMs for biosensing are used where the formation of DNA SAM followed by passivation with a small alkyl thiol is the most common approach.[31] Alternatives include coadsorption of the thiolated DNA with the small alkylthiol or the use of potential assisted SAM formation.[32−34]

Evaluating these differently prepared DNA SAMs relies on a few common facile methods. Currently techniques used to evaluate the monolayer density and quality are largely based on measuring the ensemble average, such as SPR or electrochemical redox.[2,15,21,35,36] However, these techniques lack the details needed to determine the actual characteristics of prepared monolayer. In situ AFM studies of DNA SAMs provide a single molecule view into the DNA local environment, but these can be challenging measurements that require specialized equipment.[26,37,38] Optical methods like fluorescence microscopy have also been reported, providing a more detailed picture of the surface and revealing underlying problems, such as defects and nonspecific DNA assembly, forming aggregates and clusters.[27,39,40] In addition, we have used this methodology coupled with electrochemical control of the interfacial potential to interrogate the characteristics and dynamics of the DNA SAM when prepared under a variety of conditions.[39−43] While these fluorescence imaging methods are reliable and provide spatially specific information, they are still limited to providing the average behavior on micrometer or larger regions. Coupling electrochemical control over the interfacial potential with fluorescence imaging, we have shown that using potential modulated fluorescence intensity can provide some information on the average distance between tethered DNA probes.[42,44] However, these rely on the steric limitation of DNA reorientation upon the application of negative or positive potentials and are indirectly dependent on the distance between tethered DNA.

More advanced fluorescence techniques like Forster resonance energy transfer (FRET) have the advantage of generating a detailed image of the surface as the FRET intensity has a strong dependence on the distance between the FRET pair of fluorophores. FRET has been used successfully for many years in the field of microbiology to investigate protein interaction based on the distance between labeled amino acids.[45] It has also been recently successfully applied to measure local environments of double-stranded DNA SAMs on the gold electrode.[46] FRET from molecules adsorbed to a gold surface is in competition with the quenching of the excited state of the fluorophore by the gold electrode which has a strong dependence on the separation between the fluorophore and the gold surface. This separation can be modulated by the applied potential by electrostatically repelling or attracting the tethered DNA. This results in a potential dependent fluorescence intensity and therefore FRET intensity as previously described[46] and correlated to the local environment.

Shown in this work is the application of FRET to investigate the quality of low coverage DNA SAM modification of single crystal gold bead electrodes which symmetrically display many crystallographic features. The surfaces were prepared by the potential assisted thiol exchange of DNA to provide well-defined, reproducible low DNA probe coverage surfaces with a surface specific variation in probe density. A DNA SAM was prepared with two alkylthiol modified 30-mer DNA molecule containing one of the FRET partners. The FRET intensity was compared for different donor and acceptor compositions on the surface as well as a function of the surface coverage which was dictated by the surface crystallography. The rates of DNA hybridization were investigated using fluorescence and FRET microscopy. The range of DNA surface coverages on different crystallographic regions provided a unique self-consistent comparison of the rate of hybridization on these surfaces. The influence of monolayer composition on the FRET intensity was also investigated.

EXPERIMENTAL SECTION

Materials and Methods

DNA oligomers were purchased from IDT technologies (Canada) with the sequence 5′-/HO-C6-S-S-C6-/CTG-TAT-TGA-GTT-GTA-TCG-TGT-GGT-GTA-TTT-3′, where the 3′ end is labeled with either AlexaFluor 488 (AF488) or AlexaFluor 647 (AF647). This sequence has no known secondary structures at room temperature. The thiolated DNA strands were pretreated with (100×) excess of TCEP (tris (2-carboxyethyl) phosphine-hydrochloride (98% Sigma-Aldrich), neutralized with KOH (99.99% semiconductor grade, Sigma-Aldrich), for 3 h at room temperature to break disulfide bonds. The DNA solution was filtered using GE Microspin G-50 columns. As prepared DNA solutions were kept in 10 mM TRIS (2-amino2-(hydroxymethyl)propane-1,3-diol) buffer, containing TRIS Base (Bioperformance 99.0%, Sigma-Aldrich) pH 7.5 adjusted with HNO_3 (ACS grade, AlfaAesar), in the freezer and used within 2 weeks of TCEP treatment. DNA solution used for deposition (400 nM in total DNA concentration) was made by dilution of the stock solution with an immobilization buffer (IB) composed of 10 mM TRIS (2-amino-2- (hydroxymethyl)propane-1,3-diol) buffer containing TRIS Base and TRIS HCl (Bioperformance 99.0%, Sigma-Aldrich), 100 mM NaCl (99.5% BioXtra, Sigma-Aldrich) and 25 mM $MgCl_2$ (99% Sigma-Aldrich) adjusted to pH 7.5. Millipore water (>18.3 MΩcm, Milli-Q system) was used throughout. The working glassware was washed in a 1:1 hot solution of H_2SO_4 (98% AlfaAesar) and HNO_3 (63% AlfaAesar) for at least 2 h followed by extensive rinsing in Millipore water. Aqua Regia (1:3 mixture of HNO_3 and HCl (31% AlfaAesar)) was used to etch the gold electrode surface before melting. A 1 mM solution of MCH (6-mercaptohexanol, 99% Sigma-Aldrich) was prepared in MeOH (Certified ACS, Fisher Scientific,

https://doi.org/10.1021/cbmi.3c00031
Chem. Biomed. Imaging 2023, 1, 286−296

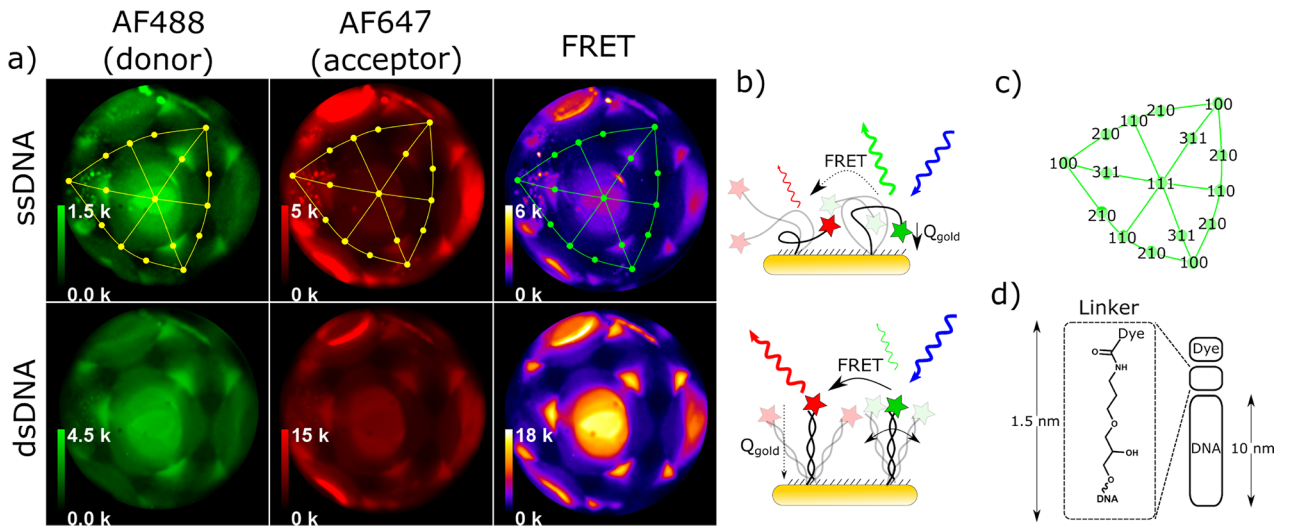

Figure 1. (a) Fluorescence images of a 50:50 AF488:AF647 ssDNA or dsDNA SAM modified single crystal bead electrode corresponding to AF488, AF647, and FRET emission. The intensity ranges for ssDNA and dsDNA SAMs were set at the same ratio (1:3) for each pair of images from the same filter cube. These images were all taken at −0.4 V/SCE. dsDNA were imaged after equilibrium with 10 nM cDNA. (b) Schematic of DNA labeled for FRET pair adsorbed on the gold electrode surface, (c) a crystallographic map illustrating the position of selected crystallographic features, and (d) schematic of a ssDNA strand, showing the 1.5 nm long linker used to attach the fluorophore to the DNA. The intensities measured for the different filter cube sets were optimized for each filter set and therefore cannot be compared directly.

Ottawa, ON, Canada). Figure 1 shows a scheme of the DNA and how the fluorophores were tethered to the DNA.

DNA SAM Deposition

Single crystal gold bead electrodes were prepared from a 1.5 cm gold wire (99.999% AlfaAesar, 1.0 mm diameter), following a previous protocol.[47] Electrodes were cleaned by immersion in Aqua Regia for 10 min, and then flame-annealed in a butane-air torch (Colibri, >99.999%). The electrodes were cleaned by cycling the potential from −1.4 to 0.6 V vs SCE, 30 times, at 50 mV/s in 0.1 M KOH (99.99%). The clean electrodes were flame-annealed and immersed in 1 mM MCH in MeOH for 90 min. Afterward, the electrode was rinsed with MeOH and water and then immersed in 60−120 μL of 400 nM solution of DNA made of a specific ratio of AF488 and AF647 in IB. The DNA SAM was prepared using potential-assisted thiol exchange (PATE) by applying +0.4 V vs SCE to the immersed electrode for 1 h. The reference electrode placed in the deposition solutionvia a glass pipet as described previously.[32] This process took place in an Eppendorf tube. The two electrode system was controlled by a potentiostat (Autolab, PGStat128N). Impedance spectra (EIS) were measured at the start and every 15 min afterward and compared to ensure consistency in the deposition. A typical $i-t$ transient is shown in Figure S1. The electrodes were stored overnight in IB at 4 °C and in the dark. Before use, the DNA SAMs were placed in IB at 40 °C for 20 min to remove nonspecifically bound DNA. The DNA SAMs prepared using PATE are stable up to 60 °C above which the {111} facets are the first to desorb.[43] Coverage was determined using $Ru(NH_3)_6Cl_3$ following the procedure outlined in ref 48. The average ssDNA coverage was ~6×10^{11} cm^{-2} which is ~5% of a densely packed DNA SAM (3×10^{13} cm^{-2})[49] (data shown in Figure S2).

In Situ Fluorescence Imaging

The DNA SAM modified electrodes were characterized with fluorescence microscopy while under electrochemical control. The electrolyte was 5 mL of 1XTAMg buffer (40 mM TRIS base and 12.5 mM $MgCl_2$, pH 8.0 adjusted with HCl), which was purged with Ar (99.998%) for at least 15 min. AC voltammetry was performed during imaging as detailed in ref 39. The electrode potential was changed by stepping the potential from +350 mV to −400 mV, in −50 mV increments, each time coming back to +350 mV base potential (potential profile in Figure S3). Each potential step lasted 6.3 s during which a fluorescence image was acquired with exposure of 5 s. The electrochemical perturbation was always done 3 times, using different filter cube sets appropriate for donor (D, AF488), acceptor (A, AF647), and FRET. The spectra for each fluorophore and the transmission spectra for each cube set are shown in Figure S4. Fluorescence images were obtained using an Olympus IX70 with a 5× objective (NA = 0.13) and an Evolve EM-CCD (Princeton). The fluorescence images shown are all 1.56 mm × 1.56 mm. The EM gain setting was optimized for donor, acceptor, and FRET channels (100, 50, and 500, respectively). After all necessary images were taken of the DNA modified surface, the monolayer was reductively desorbed, by stepping the potential from 0 to −1.4 V, in −25 mV increments. Fluorescence images acquired at the most negative potentials (before H_2 bubble formation) were used as the background which was subtracted from the fluorescence images.[39] These background images measured the leakage through the various filter cubes of the excitation light that reflect back into the objective from the gold surface. The images were analyzed using Fiji ImageJ software, as described previously.[46] Briefly, circular regions of interest (ROI) were defined for each crystallographic region (effective radii of 10 to 25 pixels, details and an example are provided in Figure S5) and the average intensity and standard deviation was measured. In the vast majority of cases, the mean and median values were within 5%. The intensities measured for the same cube can be compared, but intensities are not comparable across different imaging setups, though relative changes can be reliably compared. Complementary DNA (cDNA) was added directly to the electrochemical cell from stock kept in 1XTAMg. The hybridization kinetics was initiated by the addition of 20 μL of 2.5 μM cDNA to the electrolyte (final [cDNA] was 10 nM). The three fluorescence images (D, A, FRET) were obtained at given time intervals. Electrode was kept at OCP (which varied from −0.2 to 0 V) and Ar was gently bubbled throughout the whole hybridization process.

RESULTS AND DISCUSSION

Fluorescence Analysis of PATE Prepared DNA SAMs: Surface Crystallography, Coverage, and FRET

The ssDNA SAM was prepared on a single crystal gold bead electrode from a 50:50 mixture of AF488:AF647 labeled DNA through using the PATE method which was detailed in a previous publication.[32] Previously, we have characterized a dsDNA SAM prepared using a thiol-exchange procedure

https://doi.org/10.1021/cbmi.3c00031
Chem. Biomed. Imaging 2023, 1, 286−296

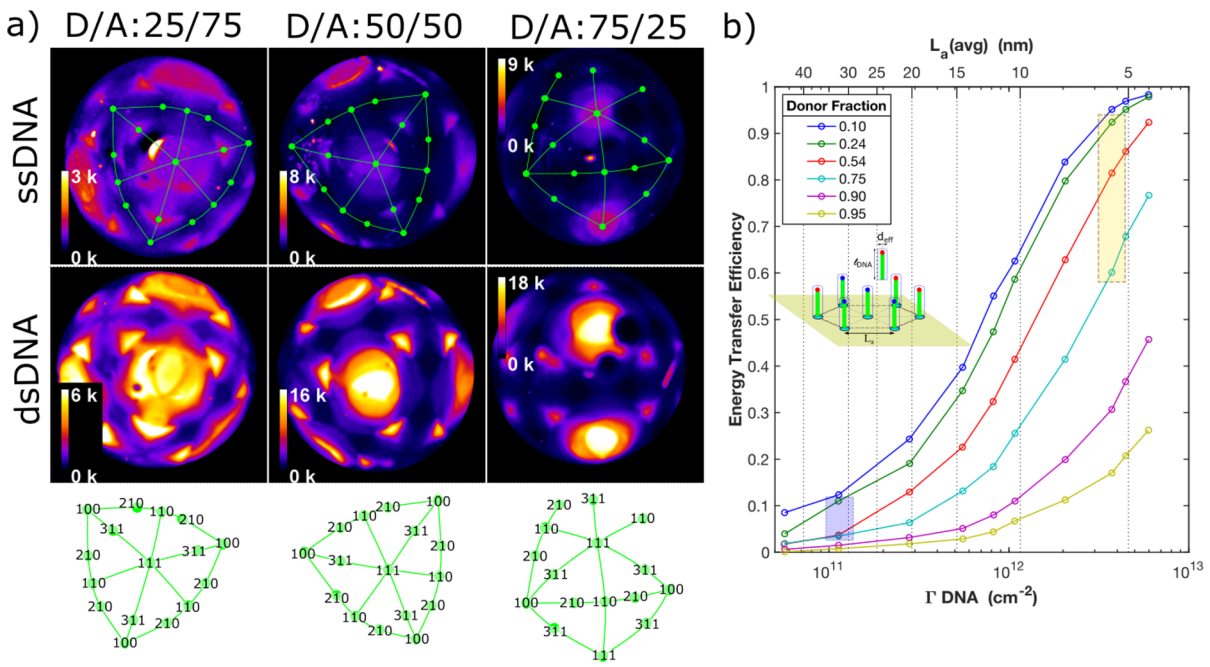

Figure 2. (a) FRET of mixtures ss and ds DNA of AF488/AF647. Top images are ssDNA and below dsDNA. From left to right (D/A) 25/75, 50/50, and 75/25. The intensity scale for the dsDNA images are represented using a scale that is twice that of the ssDNA images. The same filter cube set was used in these measurements allowing a direct comparison of the intensities. (b) ExiFRET modeling results of the FRET efficiency for a 2D system of fluorophores hexagonally arranged (see inset) as a function of Γ_{DNA} and the SAM composition. The colored bars represent the low and high coverage values that would be expected on the DNA SAM modified electrode surfaces.

without an applied potential (OCP) using the same FRET pair modified DNA to make a high coverage dsDNA SAM.[46] The dependence of FRET intensity on the AF488:AF647 ratio was shown to follow the expected trends obtained from modeling of FRET efficiency for this dsDNA SAM. The ssDNA SAMs in this work were prepared using PATE which resulted in a well-defined low ssDNA coverage that was found to be crystallographically specific where the single crystal nature of the bead electrode will be evident in the symmetry of the fluorescence images (Figure 1). Based on our previous work, the surface was mapped to show the crystallography as crystallographic triangles which connect the three low index planes ({111} − {100} − {110}). PATE creates reproducible DNA SAM covered surfaces.[32,41,42] Fluorescence images were measured for the same electrode using the three filter cubes corresponding to the donor (AF488), acceptor (AF647), and FRET shown in the top row of Figure 1 for single stranded (ss) DNA SAMs. The presence of AF488 and AF647 in the same regions on the electrode surface suggests that the fluorophore did not influence the DNA SAM preparation when done using PATE. The nonzero FRET from this mixed layer also suggests a strong colocalization of the two fluorophore labeled DNAs. The distance where FRET efficiency decreases to 50% is R_o = 5.6 nm for this FRET pair. Therefore, FRET would only be observed if they were within $2R_o$ (∼11 nm) of each other. FRET intensities are strongly correlated to the local surface density of AF488 and AF647 and showed the same crystallographically specific variation in intensity.

In general, the higher fluorescence intensities correspond to higher coverage which was observed for {111} and {311} surfaces, while lower intensities (therefore lower coverage) were observed for {100}, {110}, and {210} surfaces. The ability of the DNA to be electrostatically attracted or repelled from the electrode surface, depending on the potential is correlated to the degree of crowdedness as we have shown previously.[42] This reorientation results in a fluorescence change which can be used to compare the local conditions for the tethered DNA. In this work, a higher electrolyte ionic strength was used (as required for hybridization), so the amount of reorientation (and fluorescence intensity change) is lessened compared to previous studies. Examples of the normalized modulation in fluorescence due to applied potential is shown in Figures S6 and S7 for FRET images. Montages of the FRET images for both DNA SAMs are also shown in Figures S8 and S9. A smaller relative change in fluorescence ($\Delta F/F_{max}$) due to DNA reorientation was observed to be correlated to the larger fluorescence intensity. As modeled previously, this is a measure of the extent of crowding of the local environment around the tethered DNA.[42]

The correlation of intensity to DNA coverage is possible for the two different fluorophores, but with some limitations. The AF488 fluorophore excited state can be quenched via FRET with AF647 in addition to a distance dependent quenching by the gold surface, so a correlation to coverage is limited to cases where the FRET efficiency is low. On the other hand, AF647 intensities are only quenched by the gold surface and should in principle be directly correlated to coverage, but study of the photophysics of AF647 has shown the formation of dark states[50,51] which limits its use as a measure of coverage. This is clear when analyzing the AF647 ssDNA SAM image which shows a darker than usual central portion of the bead where the 111 facet has a significantly lower intensity when compared to the 111 facet on the side of the bead. It appears that FRET intensities do not suffer from the decrease in AF647 fluorescence due to this dark state. This can be explained recognizing that for FRET imaging, a 480 nm excitation is used which has been reported to facilitate the depopulation of the

https://doi.org/10.1021/cbmi.3c00031
Chem. Biomed. Imaging 2023, 1, 286−296

AF647 dark state back into its ground state.[50,51] The same effect is apparently occurring in these FRET images. Separate measurements of a 100% AF488 modified DNA were performed and showed a very similar pattern to the AF488 fluorescence images in the mixed composition layers suggesting that the FRET quenching of AF488 intensity may not be as significant (see Figure S10). Therefore, AF488 intensities could be used to estimate the relative coverages of DNA in different regions. Nonideal DNA SAM formations are evident at on the left side of the central {111} facet and are observed in all ssDNA fluorescence images shown in Figure 1. Interestingly, these were not observed after hybridization to dsDNA SAMs.

After equilibrating with 10 nM of cDNA for 2 h, the same fluorescence images were acquired of the presumably completely hybridized double stranded (ds)DNA SAMs. Hybridization to form dsDNA SAM fluorescence images resulted in a significantly increased intensity (Figure 1 bottom row) but the increase was not equal for all regions. After formation of dsDNA, the persistence length of DNA increases dramatically (from 2 to 50 nm)[49,52] which places the fluorophore label further from the gold surface, resulting in less quenching by gold.[42,53−55] The largest increases in AF488 and AF647 intensities are for the highest coverages {111} and {311} which also correlate with large FRET intensities. The lower coverage surfaces (e.g., {100} {110} {210}) also show increased AF488 and AF647 fluorescence when hybridized, but the FRET signal is substantially lower showing that these DNA probes are separated by >5 nm, resulting in lower FRET efficiencies. The average DNA coverage was determined using $Ru(NH_3)_6Cl_3$ ($\Gamma_{DNA} = 6 \times 10^{11}$ cm^{-2}) where the average separation would be 15 nm (assuming DNA was arranged in a uniformly distributed hexagonal array[49]). The DNA SAM is not uniformly distributed across the bead surface as shown by the strong differences in the FRET intensities indicating a wide range of separations between D and A. The use of FRET to measure the extent of hybridization on a gold surface depends greatly on the DNA local density and suggests that the average separation between DNA should be <5 nm for the largest signal change (e.g., I_{FRET} for {111} increased by >10×, while for {100} only 2× larger). This observation reflects the fact that FRET efficiency does not increase with Γ_{DNA} linearly but more dramatically when the DNA become closer than 15 nm (Figure 2b). Modeling also shows that the D:A composition of the DNA SAM can have a significant impact on the FRET efficiency and therefore indirectly on FRET intensity.

A comparison of the FRET measured from surfaces prepared with a lower or higher AF488:AF647 ratio were studied as ssDNA and dsDNA SAMs. Modeling suggests that the FRET efficiency should increase with the increase in the acceptor content in the SAM. FRET efficiency is not directly linked to the FRET intensity measured experimentally, as it is only one factor influencing FRET in addition to Γ_{DNA} and the number of donors and acceptors as well as their separation from the gold surface. Preparing reproducible DNA SAM surfaces is possible with PATE which enables a consistent assessment of the influence of SAM composition via FRET intensity.

Figure 2 shows FRET images for three different DNA SAM compositions: 25:75, 50:50, and 75:25 AF488:AF647, respectively, for both ssDNA and after hybridization (dsDNA). The largest FRET intensities were observed from the {111} and {311} surfaces for compositions containing 50% or less AF647. The DNA SAM with an excess of AF647 (acceptor) showed a more uniform FRET intensity distribution with less contrast between the surface regions. These observations are in agreement with modeling (using ExiFRET[56]) results shown in Figure 2b. SAMs with low fraction of D have a much higher efficiency for all Γ_{DNA} since there are many acceptors within R_o for FRET energy transfer. As the content of A decreases (larger fraction of D) the efficiency drops and becomes more sensitive to the distance between the D and A. For example, for a DNA SAM with a donor fraction of 0.25, the increase in FRET efficiency (from Figure 2b) when comparing low to high coverage (e.g., Γ_{DNA} increasing from 1.5×10^{11} to 4×10^{12} cm^{-2}) is 0.2 to 0.8, a 4× increase. In contrast, for a DNA SAM with a 0.75 fraction of D, the same comparison results in an increase of 10× (0.06 to 0.6). Therefore, a higher FRET contrast between low and high coverage regions is expected for higher fraction of D in the SAM, while a reduced contrast is predicted for SAMs that contain a smaller fraction of D. This is in accordance with the fluorescence images measured for both the ssDNA SAMs and dsDNA SAMs and demonstrated more quantitatively through the ratio of $\frac{I_{FRET}}{I_{AF488}}$ (Figure 3). The high coverage {111} and {311} regions show a decrease in $\frac{I_{FRET}}{I_{AF488}}$ only for the 75:25 SAM (both ss and ds DNA) while the low coverage regions ({100}, {210}, {110}) show a systematic decrease as the fraction of D decreases (the {210} surface is the lowest intensity and thus has much larger variance in the results). Both agree well with the expected behavior according to the monolayer FRET modeling and reveals a simple parameter for control of the relative FRET intensities for DNA SAMs with differing Γ_{DNA}.

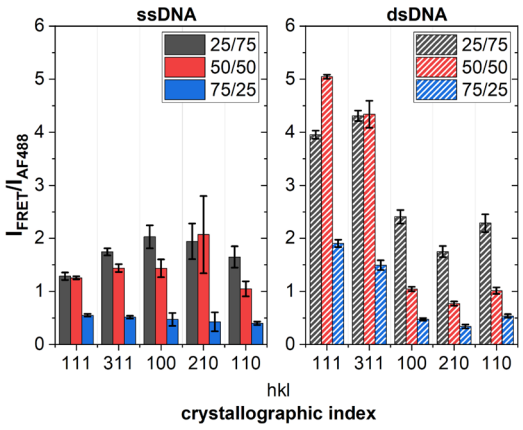

Figure 3. Ratios of FRET intensity divided by intensity of the donor for ssDNA and dsDNA monolayers for the three compositions of DNA SAM (e.g., ratio of AF488/AF647). I_{FRET}/I_{AF488} represents ratio of acceptors excited by energy transfer to the donor that did not participate in energy transfer. Error bars represent 1 standard deviation of the intensities measured from the ROI. The relative values of these ratios can be compared, but the absolute value has no significance given the image intensities were measured using different settings for AF488 and FRET.

The composition of the FRET active DNA SAM can control the extent of the FRET signal increase resulting from hybridization of the ssDNA SAM. This is important as most DNA SAMs are prepared on polycrystalline gold electrode surfaces and would have a range of coverages depending on the preparation conditions. For a DNA SAM with high fraction of donor, this would result in a FRET signal that would be

https://doi.org/10.1021/cbmi.3c00031
Chem. Biomed. Imaging 2023, 1, 286−296

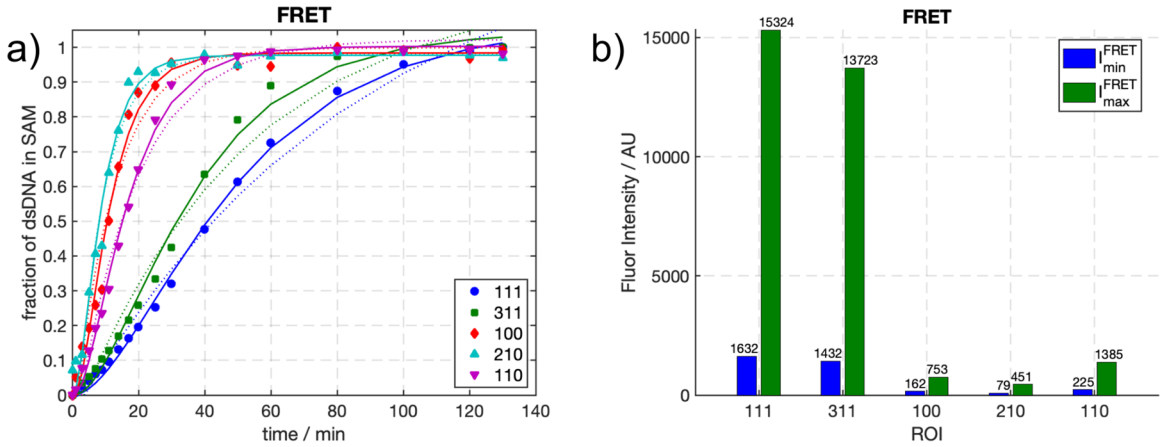

Figure 4. (a) FRET normalized fluorescence intensity for the 50:50 AF488:AF647 DNA SAM taken at time after addition of 10 nM of cDNA. The lines are the fitted results for the first order (dashed) and second order (solid) rate expressions; (b) the FRET intensity for selected surfaces.

dominated by the high coverage regions. Decreasing the donor fraction would increase the contribution to the average FRET intensity of the low coverage regions. The differences in the hybridization rates is a strong function of Γ_{DNA}[17,18,24] and larger FRET signals may not be the sole important parameter for optimizing DNA SAM based sensors as shown next.

Hybridization Kinetics

50:50 AF488:AF647 DNA SAM. Literature shows that surface bound DNA has a much slower hybridization rate than the same sequence in solution.[20−24] The surface offers a significant impediment to the bound DNA which constrains its ability to facilitate the initial nucleation process that initiates hybridization with cDNA in solution (e.g., formation of an initial base pairing of 4 or more, and then a zipping up).[22,24,26] The rate of DNA hybridization to a surface bound probe can be modeled using a first order Langmuir fit, though deviations were observed suggesting heterogeneous binding site energies.[21,23] In addition, it was shown that for coverages of $\Gamma = 5 \times 10^{12}$ cm^{-2}, hybridization was rapid (<1 h) but not always complete suggesting again a heterogeneous probe environment where some ssDNA probe were not easily accessible.[17,18,21,23] Fluorescence imaging can also be used to monitor the extent of DNA hybridization. Furthermore, in our studies, the rate of ssDNA probe hybridization can be directly and self-consistently measured from each ROI on the electrode surface representing a range of Γ_{DNA}. As shown above, FRET intensity increases since hybridized DNA (dsDNA) has a larger persistence length and will extend further from the surface into solution, decreasing the quenching by gold. An estimate of the fraction of ssDNA SAM that has been hybridized can be determined from the FRET intensity once converted into a parameter that is linear with the fraction of dsDNA such as the average separation of the fluorophore from the gold surface.

The average distance (d_{avg}) between the gold surface and the fluorophore can be determined from the fluorescence intensity (I) since it depends on the cube of the separation ($I \propto d^3$).[42] The DNA probes were assumed to be either ss or ds with a corresponding characteristic separation of the fluorophore from the gold surface of either d_{ss} and d_{ds}. This two state model does not include any intermediate orientation or conformations of the DNA in the SAM. In this simple model, the fraction of probes hybridized (f_{ds}) at any time t can be determined using

$$f_{ds}(t) = \frac{d_{avg}(t) - d_{ss}}{d_{ds} - d_{ss}} \quad (1)$$

where $d_{avg}(t) = d_{ss}\Gamma_{ss}(t) + d_{ds}\Gamma_{ds}(t)$ and $\Gamma_{ss}(t) + \Gamma_{ds}(t) = \Gamma_{total}$ which is the total number of bound DNA probes. This equation can be rewritten to use fluorescence intensities as

$$f_{ds}(t) = \frac{\sqrt[3]{I(t)} - \sqrt[3]{I_{ss}}}{\sqrt[3]{I_{ds}} - \sqrt[3]{I_{ss}}} \quad (2)$$

The rate of hybridization should be the same for both fluorescently labeled ssDNA probes (AF488 and AF647), so the formation of dsDNA in the SAM can be described by a first order Langmuir adsorption rate (assuming a negligible amount of dehybridization and no mass transport limitations)

$$\frac{df_{ds}}{dt} = kc_{cDNA}(1 - f_{ds}(t)) \quad (3)$$

Integration results in a first order Langmuir adsorption rate expression

$$f_{ds} = 1 - \exp(-k_{eff}t) \quad (4)$$

where k_{eff} is the effective rate constant for hybridization. This derivation assumes that the hybridization process is not impeded by neighboring ssDNA or dsDNA.[21] The veracity of this assumption will depend on Γ_{DNA} which is estimated on these single crystal gold beads when prepared by PATE, to range from 1.5×10^{11} to 2×10^{12} cm^{-2} depending on the crystallographic region analyzed.

FRET can be used to monitor hybridization. An increase in FRET will require two hybridized partners that are near enough to each other (e.g., within $2R_o$). No significant FRET will be measured from a ssDNA−dsDNA pair since they will be separated by $>2R_o$ or >10 nm. The rate of hybridization as measured using FRET can be described as a second order process, and assuming the hybridization rates for AF488 and AF647 labeled DNA are the same, then

$$f_{ds}^{FRET} = (1 - \exp(-k't))^2 \quad (5)$$

The assumption about the rates of hybridization for the two fluorophore labeled ssDNA probes should be reliable since both have the same 30mer sequence. In addition to a decrease in quenching by the gold surface, this increased separation

https://doi.org/10.1021/cbmi.3c00031
Chem. Biomed. Imaging 2023, 1, 286−296

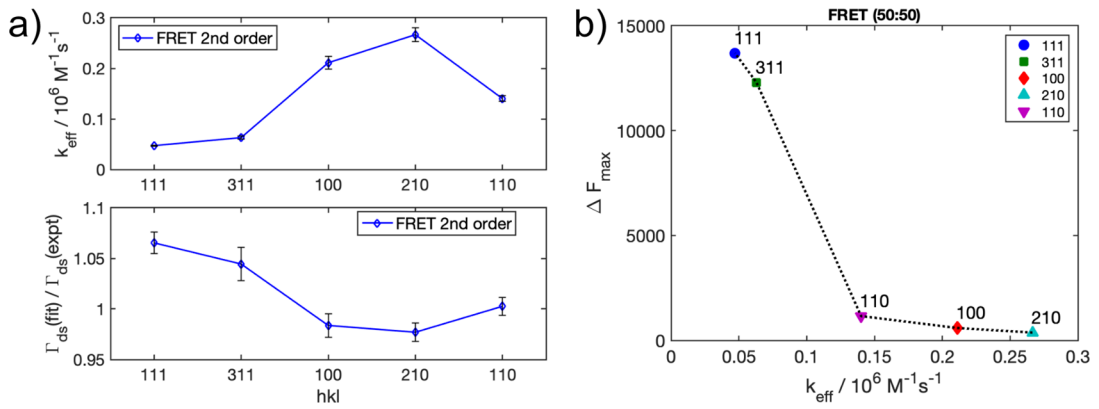

Figure 5. (a) The model parameters (k_{eff} and relative coverage correction) from fitting the second order model to the FRET data from the 50:50 AF488:AF647 DNA SAM. (b) A comparison of the maximum change in FRET fluorescence upon hybridization to the rate of hybridization illustrating the influence of coverage on the rate of hybridization.

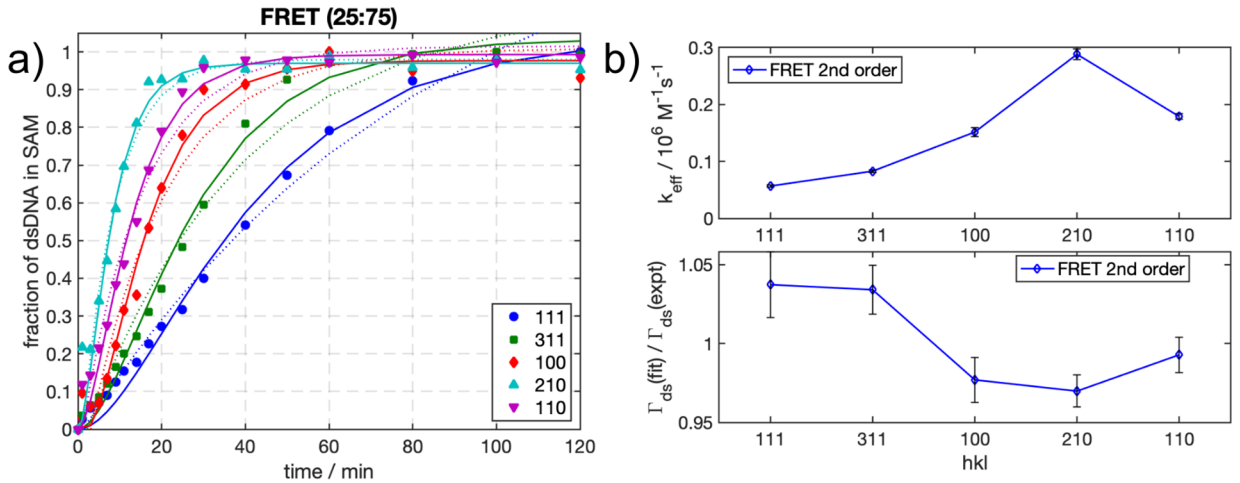

Figure 6. (a) Normalized FRET fluorescence intensity for a 25:75 AF488:AF647 DNA SAM measured after addition of 10 nM of cDNA. The lines are the fitted results for the first order (dashed) and second order (solid) rate expressions. (b) The fitted parameters (k_{eff} and relative coverage correction).

from the gold will increase the mobility of the tethered DNA resulting in an increase in FRET efficiency as the end-labeled tethered dsDNA should, on average, be closer together than for the same ssDNA SAMs.

In our system, the use of a single crystal bead electrode provides the unique opportunity to directly investigate the role of surface coverage in the rate of hybridization in a self-consistent manner. Figure 4a shows the normalized change in FRET intensity for five different ROIs during a hybridization process with 10 nM of cDNA added into the electrolyte at t = 0. Figure 4b shows the intensities for each surface before and after hybridization. The time required to achieve f_{ds} = 1 strongly depended on the coverage of the DNA probe. The lower coverage surfaces ({100}, {110}, {210}) saturated after 20 min. The {111} and {311} surfaces took about 2 h to completely saturate. The relative increase in FRET intensities were also larger for the {111} and {311} surfaces, reflecting the large increase in FRET efficiency with coverage (Figure 2b). The FRET results are fit to both kinetic models (eqs 4 and 5) with the data better explained using the latter model (since the number of fitted parameters are the same, comparing the coefficient of determination (R^2) (given in Table S1) is valid (0.96 vs 0.99 on average)).

Figure 5 show the parameters extracted from the fitting to the second order models. A correction factor for the maximum coverage (Γ_{ds}(fit)/Γ_{ds}(expt)) and the rate constant (k_{eff}) were both parameters in the fit in addition to a delay reflecting the fact that the images were not acquired at the same time (fitting results in SI Figures S11 and S12). As expected, the higher coverage ROIs show the slowest hybridization rate (k_{eff} = 5 × 10^4 M^{-1} s^{-1}) which are 5× smaller than the lowest coverage region ({210} k_{eff} = 2.7 × 10^5 M^{-1} s^{-1}). These rates are comparable to the DNA hybridization rates for a 25mer found in solution (10 × 10^4 M^{-1} s^{-1}) and faster than the same sequence on gold surface (0.5 × 10^4 M^{-1} s^{-1} for a Γ_{ssDNA} ≈ 5 × 10^{12} DNA cm^{-2}) as measured using SPR.[21] Comparing to results which used a different sequence can be problematic, since hybridization rates measured in solution depend on the sequence and were found to range over 2 orders of magnitude for the same number of bases.[57]

The k_{eff} was correlated to the extent of reorientation ($\Delta F/F_{max}$) measured for the ssDNA as well for the dsDNA SAM as shown in Figure S13. This confirms that the estimate of the amount of free space available to the tethered DNA is correlated and has a significant impact on the rate of hybridization. The veracity of normalizing using the 120 min FRET intensity can be evaluated using $\frac{\Gamma_{ds}(\text{fit})}{\Gamma_{ds}(\text{expt})}$. The low

https://doi.org/10.1021/cbmi.3c00031
Chem. Biomed. Imaging 2023, 1, 286−296

coverage regions show they were fully hybridized $\left(\frac{\Gamma_{ds}(\text{fit})}{\Gamma_{ds}(\text{expt})} = 0.95 \text{ to } 1\right)$, while the high coverage regions fit better if the estimate for the maximum coverage was higher $\left(\frac{\Gamma_{ds}(\text{fit})}{\Gamma_{ds}(\text{expt})} > 1\right)$ than estimated suggesting that the interfaces were not at equilibrium after 120 min, or that the model used to estimate the fraction of dsDNA was not accurate for these high coverage regions.

The rate of hybridization measured using FRET can be compared by considering the increase in the fluorescence signal upon hybridization (ΔF) as shown in Figure 5b. The relative increase in FRET fluorescence is strongly correlated to the rate of hybridization showing the influence of Γ_{DNA} on both parameters. For a 50:50 DNA SAM, the FRET intensity increase due to hybridization is 15× larger for the higher packing density. This dramatic increase in FRET highlights the bias present in an average measurement of intensity, favoring regions where the average separation is $<2R_o$ (or $\Gamma > 10^{12}$ cm^{-2} for this FRET pair). This comes at a cost of a significantly slower rate of hybridization in agreement with other studies of surface hybridization rates. As demonstrated with the FRET modeling, the efficiency of the FRET process can be manipulated by changing the AF488:AF647 (D:A) ratio.

25:75 AF488:AF647 DNA SAM. To understand the influence of the composition of the mixed DNA SAM on FRET hybridization measurements, a 25:75 AF488:AF647 ssDNA SAM was used to study hybridization following the same approach as the 50:50 SAM. These results are given in Figure 6 with the FRET intensities shown in Figure S14. As shown previously, the decrease in AF488 content improves the FRET efficiency, though not necessarily resulting in an increase in the FRET intensity. The composition of the SAM appears to control the relative increase in FRET upon hybridization. Monitoring normalized FRET intensity increases with time and treating the data in the same way as described for the 50:50 SAM shows the same general trends: (1) the lower coverage regions completed hybridization after 20 min while the higher coverage {111} and {311} ROIs required more than 2 h, (2) the FRET intensities were best described by the second order model, (3) the k_{eff} determined were very similar to the 50:50 sample. The consistency in these hybridization results showed that the FRET hybridization measurement is not dependent on the DNA SAM composition. In addition, the preparation method used for these DNA SAMs resulted in surfaces which performed similarly showing the benefits of the preparing reproducible DNA SAMs using PATE.

The behavior of these two DNA SAMs of different compositions is compared in Figure 7 by analyzing the k_{eff} rate constants and the relative increase in FRET intensity due to hybridization $\left(\frac{F_{ds} - F_{ss}}{F_{ss}} = \Delta F/F_{ss}\right)$. The 50:50 FRET results show a dependence between the rate of hybridization and coverage, with the largest changes in FRET resulting from higher coverage regions, though with a smaller k_{eff}. Changing the composition to 25:75 D:A resulted in a relatively constant relative increase in FRET intensity upon hybridization for all values of k_{eff}. This highlights the influence of DNA SAM composition on the properties of the sensing surface, providing guidance on how the parameters (coverage, composition) can be manipulated to achieve the desired rate of hybridization and the intensity increase for a binding/hybridization event.

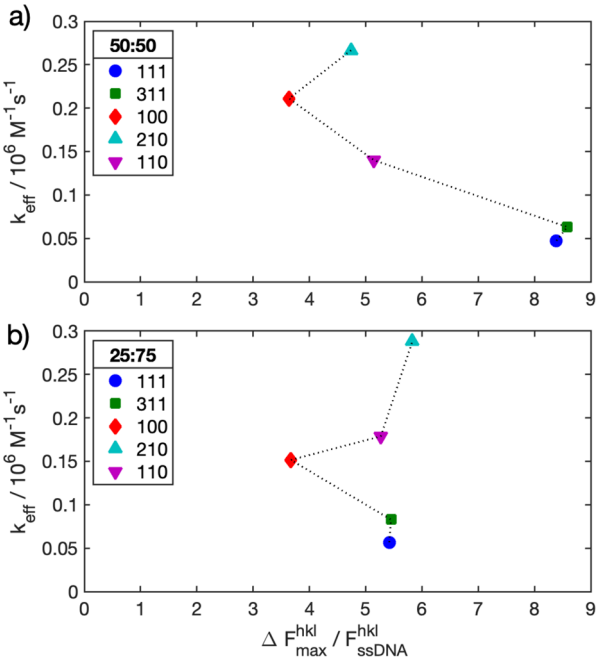

Figure 7. Comparison of the relative increase in FRET intensity ($\Delta F/F_{ss}$) for each crystallographic region and the rate of hybridization for the 50:50 D:A DNA SAM (closed symbol) and the 25:75 D:A DNA SAM (open symbols). Lines were added to guide the eye.

Further study is required to improve the low coverage FRET intensity response such as selecting a FRET pair that has a larger R_o or increasing the length of the linkage between the distal end of the DNA and the fluorophore.

CONCLUSION

Förster resonance energy transfer (FRET) was used to study DNA SAMs labeled with fluorophores that were prepared on a single crystal gold bead electrode using potential-assisted thiol-exchange. A direct assessment of the crowding of the molecular arrangement of the probes on the surface was possible using FRET microscopy. A range of DNA coverage exists on these electrodes (from 1.5×10^{11} to 2×10^{12} cm^{-2}) which impacted the FRET signals revealing that FRET can provide a measure of the local DNA SAM arrangement on each crystallographic region of interest providing a direct assessment of the probe environment. A large FRET signal was measured for high coverage vs low coverage regions, and the FRET intensity was shown to depend on the composition of the SAM and the local coverage in correspondence with modeling. The FRET intensity also dramatically increased for DNA SAMs when hybridized. This increase in FRET enabled a kinetic analysis of the surface-based hybridization process since hybridization increases the average distance between the fluorophore label and the gold electrode surface and decreases the distance between the donor (D) and acceptor (A), both resulting in an increase FRET fluorescence intensity. The FRET increase was modeled using a second order Langmuir adsorption rate equation reflecting the fact that for FRET to occur, both D and A labeled DNA need to become hybridized. The self-consistent analysis of the hybridization on low and high coverage regions on the same electrode showed that the low coverage regions achieved full hybridization 5× faster than the higher coverage regions. The low coverage surface regions have hybridization rates similar to those typically found in solution but are often

https://doi.org/10.1021/cbmi.3c00031
Chem. Biomed. Imaging 2023, 1, 286−296

challenging to measure on a surface. We demonstrated that our FRET method enabled measurement of surface hybridization in low coverage DNA SAMs. Changing the composition of the DNA SAM was found to control the relative increase in FRET intensity from each region of interest due to hybridization weakly dependent on probe density or the rate of hybridization. This work shows that measurements of FRET on a modified electrode surface can be optimized by controlling the coverage and the composition of the DNA SAM facilitating FRET detection of biorecognition or analysis. Further improvements in using FRET to detect hybridization will require optimizing the FRET parameters for low coverage surfaces (using a FRET pair with larger R_0 (e.g., >5 nm), or modifying DNA with a fluorophore attached by a longer tether would increase the range of interaction/energy transfer) and optimizing the D:A ratio of the mixed DNA SAM to achieve more uniform response from the typical multicrystalline sensor surface.

■ ASSOCIATED CONTENT

Supporting Information

The Supporting Information is available free of charge at https://pubs.acs.org/doi/10.1021/cbmi.3c00031.

> Example of electrochemical data for a typical potential-assisted thiol exchange (PATE) preparation of a DNA SAM; Example of a measurement of DNA coverage; Potential profile applied for measuring changes in fluorescence due to DNA reorientation; Details of the AF488 and AF647 spectra and filter sets used for acquisition of the three fluorescence images; Example of ROI selections; Fluorescence intensity change with potential controlled reorientation of DNA; Montage of the FRET images during hybridization; Fluorescence images for both ssDNA and dsDNA SAMs composed of only AF488 modified DNA; Results for fitting the FRET intensity during hybridization; FRET intensities of the 25:75 AF488:AF647 DNA SAMs (PDF)

■ AUTHOR INFORMATION

Corresponding Author

Dan Bizzotto − *AMPEL and Department of Chemistry, University of British Columbia, Vancouver, British Columbia V6T 1Z4, Canada;* orcid.org/0000-0002-2176-6799; Email: bizzotto@chem.ubc.ca

Authors

Adrian Jan Grzędowski − *AMPEL and Department of Chemistry, University of British Columbia, Vancouver, British Columbia V6T 1Z4, Canada;* orcid.org/0000-0001-7847-0094

Tianxiao Ma − *AMPEL and Department of Chemistry, University of British Columbia, Vancouver, British Columbia V6T 1Z4, Canada;* orcid.org/0000-0002-3982-0079

Complete contact information is available at: https://pubs.acs.org/10.1021/cbmi.3c00031

Notes

The authors declare no competing financial interest.

■ ACKNOWLEDGMENTS

This research was supported by grants from the Canadian Natural Sciences and Engineering Research Council (NSERC) to D.B. (RGPIN 2016-05528 and RGPIN-2022-04419) and from New Frontiers in Research Fund/Exploration (NFRFE-2019-01105). Prof. R. Fernandez (UBC) and A. Mahey (UBC) provided feedback and helpful suggestions for this work.

■ REFERENCES

(1) Ye, X.; Wang, X.; Kong, Y.; Dai, M.; Han, D.; Liu, Z. FRET Modulated Signaling: A Versatile Strategy to Construct Photoelectrochemical Microsensors for In Vivo Analysis. *Angew. Chem. - Int. Ed.* **2021**, *60*, 11774−11778.

(2) Trotter, M.; Borst, N.; Thewes, R.; von Stetten, F. Review: Electrochemical DNA sensing − Principles, commercial systems, and applications. *Biosens. Bioelectron.* **2020**, *154*, 112069.

(3) Pellitero, M. A.; Shaver, A.; Arroyo-Currás, N. Critical Review-Approaches for the Electrochemical Interrogation of DNA-Based Sensors: A Critical Review. *J. Electrochem. Soc.* **2020**, *167*, 037529.

(4) Kim, J.; Park, J.; Park, S.; Seo, J.; Kwon, J.; Lee, H.; Kim, S.; Yang, H. Surface-Plasmonic-Field-Induced Photoredox Catalysis and Mediated Electron Transfer for Washing Free DNA Detection. *Angew. Chem. - Int. Ed.* **2020**, *59*, 19202−19208.

(5) Dauphin-Ducharme, P.; Yang, K.; Arroyo-Currás, N.; Ploense, K. L.; Zhang, Y.; Gerson, J.; Kurnik, M.; Kippin, T. E.; Stojanovic, M. N.; Plaxco, K. W. Electrochemical Aptamer-Based Sensors for Improved Therapeutic Drug Monitoring and High-Precision, Feedback-Controlled Drug Delivery. *ACS Sens* **2019**, *4*, 2832−2837.

(6) Zhang, X.; Hu, Y.; Yang, X.; Tang, Y.; Han, S.; Kang, A.; Deng, H.; Chi, Y.; Zhu, D.; Lu, Y. FÖrster resonance energy transfer (FRET)-based biosensors for biological applications. *Biosens. Bioelectron.* **2019**, *138*, 111314.

(7) Labib, M.; Sargent, E. H.; Kelley, S. O. Electrochemical Methods for the Analysis of Clinically Relevant Biomolecules. *Chem. Rev.* **2016**, *116*, 9001−9090.

(8) Peterson, E. M.; Manhart, M. W.; Harris, J. M. Single-Molecule Fluorescence Imaging of Interfacial DNA Hybridization Kinetics at Selective Capture Surfaces. *Anal. Chem.* **2016**, *88*, 1345−1354.

(9) Tang, Y.; Ge, B.; Sen, D.; Yu, H. Z. Functional DNA switches: rational design and electrochemical signaling. *Chem. Soc. Rev.* **2014**, *43*, 518−529.

(10) Rhouati, A.; Marty, J.-L.; Vasilescu, A. Electrochemical biosensors combining aptamers and enzymatic activity: Challenges and analytical opportunities. *Electrochim. Acta* **2021**, *390*, 138863.

(11) Langer, A.; Kaiser, W.; Svejda, M.; Schwertler, P.; Rant, U. Molecular Dynamics of DNA-Protein Conjugates on Electrified Surfaces: Solutions to the Drift-Diffusion Equation. *J. Phys. Chem. B* **2014**, *118*, 597−607.

(12) Kang, D.; Zuo, X.; Yang, R.; Xia, F.; Plaxco, K. W.; White, R. J. Comparing the Properties of Electrochemical-Based DNA Sensors Employing Different Redox Tags. *Anal. Chem.* **2009**, *81*, 9109−9113.

(13) Esteban Fernandez de Avila, B.; Watkins, H. M.; Pingarron, J. M.; Plaxco, K. W.; Palleschi, G.; Ricci, F. Determinants of the Detection Limit and Specificity of Surface-Based Biosensors. *Anal. Chem.* **2013**, *85*, 6593−6597.

(14) Ricci, F.; Vallée-Belisle, A.; Simon, A. J.; Porchetta, A.; Plaxco, K. W. Using Nature's "Tricks" To Rationally Tune the Binding Properties of Biomolecular Receptors. *Acc. Chem. Res.* **2016**, *49*, 1884−1892.

(15) Dauphin-Ducharme, P.; Plaxco, K. W. Maximizing the Signal Gain of Electrochemical-DNA Sensors. *Anal. Chem.* **2016**, *88*, 11654−11662.

(16) Sykes, K. S.; White, R. J. Effects of Nucleic Acid Structural Heterogeneity on the Electrochemistry of Tethered Redox Molecules. *Langmuir* **2022**, *38*, 7322−7330.

(17) Peterson, A. W.; Heaton, R. J.; Georgiadis, R. M. The effect of surface probe density on DNA hybridization. *Nucleic Acids Res.* **2001**, *29*, 5163−5168.
(18) Biagiotti, V.; Porchetta, A.; Desiderati, S.; Plaxco, K. W.; Palleschi, G.; Ricci, F. Probe accessibility effects on the performance of electrochemical biosensors employing DNA monolayers. *Anal. Bioanal. Chem.* **2012**, *402*, 413−421.
(19) Ravan, H.; Kashanian, S.; Sanadgol, N.; Badoei-Dalfard, A.; Karami, Z. Strategies for optimizing DNA hybridization on surfaces. *Anal. Biochem.* **2014**, *444*, 41−46.
(20) Gong, P.; Levicky, R. DNA surface hybridization regimes. *Proc. Natl. Acad. Sci. U. S. A.* **2008**, *105*, 5301−5306.
(21) Gao, Y.; Wolf, L. K.; Georgiadis, R. M. Secondary structure effects on DNA hybridization kinetics: a solution versus surface comparison. *Nucleic Acids Res.* **2006**, *34*, 3370−3377.
(22) Monserud, J. H.; Schwartz, D. K. Mechanisms of Surface-Mediated DNA Hybridization. *ACS Nano* **2014**, *8*, 4488−4499.
(23) Vanjur, L.; Carzaniga, T.; Casiraghi, L.; Chiari, M.; Zanchetta, G.; Buscaglia, M. Non-Langmuir Kinetics of DNA Surface Hybridization. *Biophys. J.* **2020**, *119*, 989−1001.
(24) Treasurer, E.; Levicky, R. How Surfaces Affect Hybridization Kinetics. *J. Phys. Chem. B* **2021**, *125*, 2976−2986.
(25) Tawa, K.; Knoll, W. Mismatching base-pair dependence of the kinetics of DNA−DNA hybridization studied by surface plasmon fluorescence spectroscopy. *Nucleic Acids Res.* **2004**, *32*, 2372−2377.
(26) Gu, Q.; Cao, H. H.; Zhang, Y.; Wang, H.; Petrek, Z. J.; Shi, F.; Josephs, E. A.; Ye, T. Toward a Quantitative Relationship between Nanoscale Spatial Organization and Hybridization Kinetics of Surface Immobilized Hairpin DNA Probes. *ACS Sens* **2021**, *6*, 371−379.
(27) Meunier, A.; Triffaux, E.; Bizzotto, D.; Buess-Herman, C.; Doneux, T. In-Situ Fluorescence Microscopy Study of the Interfacial Inhomogeneity of DNA Mixed Self-Assembled Monolayers at Gold Electrodes. *ChemElectroChem.* **2015**, *2*, 434−442.
(28) Yu, Z. L.; Yang, C. W. T.; Triffaux, E.; Doneux, T.; Turner, R. F. B.; Bizzotto, D. Measuring and Remediating Nonspecific Modifications of Gold Surfaces Using a Coupled in Situ Electrochemical Fluorescence Microscopic Methodology. *Anal. Chem.* **2017**, *89*, 886−894.
(29) Soleymani, L.; Fang, Z.; Sun, X.; Yang, H.; Taft, B.; Sargent, E.; Kelley, S. Nanostructuring of Patterned Microelectrodes To Enhance the Sensitivity of Electrochemical Nucleic Acids Detection. *Angew. Chem-ger Edit* **2009**, *121*, 8609−8612.
(30) Arroyo-Currás, N.; Scida, K.; Ploense, K. L.; Kippin, T. E.; Plaxco, K. W. High Surface Area Electrodes Generated via Electrochemical Roughening Improve the Signaling of Electrochemical Aptamer-Based Biosensors. *Anal. Chem.* **2017**, *89*, 12185−12191.
(31) Herne, T. M.; Tarlov, M. J. Characterization of DNA Probes Immobilized on Gold Surfaces. *J. Am. Chem. Soc.* **1997**, *119*, 8916−8920.
(32) Leung, K. K.; Gaxiola, A. D.; Yu, H.-Z.; Bizzotto, D. Tailoring the DNA SAM surface density on different surface crystallographic features using potential assisted thiol exchange. *Electrochim. Acta* **2018**, *261*, 188−197.
(33) Jambrec, D.; Gebala, M.; La Mantia, F.; Schuhmann, W. Potential-Assisted DNA Immobilization as a Prerequisite for Fast and Controlled Formation of DNA Monolayers. *Angew. Chem. - Int. Ed.* **2015**, *54*, 15064−15068.
(34) Doneux, T.; DeRache, A.; Triffaux, E.; Meunier, A.; Steichen, M.; Buess-Herman, C. Optimization of the Probe Coverage in DNA Biosensors by a One - Step Coadsorption Procedure. *ChemElectroChem.* **2014**, *1*, 147−157.
(35) Peterson, A. W.; Wolf, L. K.; Georgiadis, R. M. Hybridization of Mismatched or Partially Matched DNA at Surfaces. *J. Am. Chem. Soc.* **2002**, *124*, 14601−14607.
(36) Lubin, A. A.; Hunt, B. V. S.; White, R. J.; Plaxco, K. W. Effects of Probe Length, Probe Geometry, and Redox-Tag Placement on the Performance of the Electrochemical E-DNA Sensor. *Anal. Chem.* **2009**, *81*, 2150−2158.
(37) Josephs, E. A.; Ye, T. A Single-Molecule View of Conformational Switching of DNA Tethered to a Gold Electrode. *J. Am. Chem. Soc.* **2012**, *134*, 10021−10030.
(38) Gu, Q.; Josephs, E. A.; Ye, T. Hybridization and self-assembly behaviors of surface-immobilized DNA in close proximity: A single-molecule perspective. *Aggregate* **2022**, *3*, No. e186.
(39) Casanova-Moreno, J.; Yu, Z. L.; Massey-Allard, J.; Ditchburn, B.; Young, J. F.; Bizzotto, D. *Luminescence in Electrochemistry*; Springer International Publishing: Cham, pp 21−77.
(40) Murphy, J. N.; Cheng, A. K. H.; Yu, H. Z.; Bizzotto, D. On the Nature of DNA Self-Assembled Monolayers on Au: Measuring Surface Heterogeneity with Electrochemical in Situ Fluorescence Microscopy. *J. Am. Chem. Soc.* **2009**, *131*, 4042−4050.
(41) Leung, K. K.; Yu, H.-Z.; Bizzotto, D. Electrodepositing DNA Self-Assembled Monolayers on Au: Detailing the Influence of Electrical Potential Perturbation and Surface Crystallography. *ACS Sens* **2019**, *4*, 513−520.
(42) Leung, K. K.; Martens, I.; Yu, H. Z.; Bizzotto, D. Measuring and Controlling the Local Environment of Surface-Bound DNA in Self-Assembled Monolayers on Gold When Prepared Using Potential-Assisted Deposition. *Langmuir* **2020**, *36*, 6837−6847.
(43) Ma, T.; Bizzotto, D. Improved Thermal Stability and Homogeneity of Low Probe Density DNA SAMs Using Potential-Assisted Thiol-Exchange Assembly Methods. *Anal. Chem.* **2021**, *93*, 15973−15981.
(44) Ma, T.; Grzędowski, A. J.; Doneux, T.; Bizzotto, D. Redox-Controlled Energy Transfer Quenching of Fluorophore-Labeled DNA SAMs Enables In Situ Study of These Complex Electrochemical Interfaces. *J. Am. Chem. Soc.* **2022**, *144*, 23428−23437.
(45) Sun, Y.; Wallrabe, H.; Seo, S. A.; Periasamy, A. FRET Microscopy in 2010: The Legacy of Theodor Förster on the 100th Anniversary of his Birth. *ChemPhysChem* **2011**, *12*, 462−474.
(46) Verhaven, A.; Doneux, T.; Bizzotto, D. Application of FRET Microscopy to the Study of the Local Environment and Dynamics of DNA SAMs on Au Electrodes. *Langmuir* **2018**, *34*, 14802−14810.
(47) Yu, Z. L.; Casanova-Moreno, J.; Guryanov, I.; Maran, F.; Bizzotto, D. Influence of Surface Structure on Single or Mixed Component Self-Assembled Monolayers via in Situ Spectroelectrochemical Fluorescence Imaging of the Complete Stereographic Triangle on a Single Crystal Au Bead Electrode. *J. Am. Chem. Soc.* **2015**, *137*, 276−288.
(48) Ge, B.; Huang, Y.-C.; Sen, D.; Yu, H.-Z. Electrochemical investigation of DNA-modified surfaces: From quantitation methods to experimental conditions. *J. Electroanal. Chem.* **2007**, *602*, 156−162.
(49) Li, Z.; Niu, T.; Zhang, Z.; Chen, R.; Feng, G.; Bi, S. Exploration of the specific structural characteristics of thiol-modified single-stranded DNA self-assembled monolayers on gold by a simple model. *Biosens. Bioelectron.* **2011**, *26*, 4564−4570.
(50) Herdly, L.; Tinning, P. W.; Geiser, A.; Taylor, H.; Gould, G. W.; Linde, S. v. d. Benchmarking Thiolate-Driven Photoswitching of Cyanine Dyes. *J. Phys. Chem. B* **2023**, *127*, 732−741.
(51) Vandenberk, N.; Barth, A.; Borrenberghs, D.; Hofkens, J.; Hendrix, J. Evaluation of Blue and Far-Red Dye Pairs in Single-Molecule Förster Resonance Energy Transfer Experiments. *J. Phys. Chem. B* **2018**, *122*, 4249−4266.
(52) Hagerman, P. J. Flexibility of DNA. *Annu. Rev. Biophys. Biophys. Chem.* **1988**, *17*, 265−286.
(53) Rant, U.; Arinaga, K.; Fujita, S.; Yokoyama, N.; Abstreiter, G.; Tornow, M. Dynamic Electrical Switching of DNA Layers on a Metal Surface. *Nano Lett.* **2004**, *4*, 2441−2445.
(54) Kaiser, W.; Rant, U. Conformations of End-Tethered DNA Molecules on Gold Surfaces: Influences of Applied Electric Potential, Electrolyte Screening, and Temperature. *J. Am. Chem. Soc.* **2010**, *132*, 7935−7945.
(55) Casanova-Moreno, J.; Bizzotto, D. A Method for Determining the Actual Rate of Orientation Switching of DNA Self-Assembled Monolayers Using Optical and Electrochemical Frequency Response Analysis. *Anal. Chem.* **2015**, *87*, 2255−2263.

https://doi.org/10.1021/cbmi.3c00031
Chem. Biomed. Imaging 2023, 1, 286−296

(56) Deplazes, E.; Jayatilaka, D.; Corry, B. ExiFRET: flexible tool for understanding FRET in complex geometries. *J. Biomed Opt* **2012**, *17*, 011005.
(57) Hata, H.; Kitajima, T.; Suyama, A. Influence of thermodynamically unfavorable secondary structures on DNA hybridization kinetics. *Nucleic Acids Res.* **2018**, *46*, 782−791.

https://doi.org/10.1021/cbmi.3c00031
Chem. Biomed. Imaging 2023, 1, 286−296